RAC: Reconfiguration-Assisted Charging in Large-Scale Lithium-Ion Battery Systems

Liang He, *Member, IEEE*, Linghe Kong, *Member, IEEE*, Siyu Lin, *Member, IEEE*,
Shaodong Ying, *Member, IEEE*, Yu (Jason) Gu, *Member, IEEE*,
Tian He, *Senior Member, IEEE*, and Cong Liu, *Member, IEEE*

Abstract—Large-scale lithium-ion battery packs are widely adopted in systems such as electric vehicles and energy backup in power grids. Due to factors such as manufacturing difference and heterogeneous discharging conditions, cells in the battery pack may have different statuses, such as diverse voltage levels. This cell diversity is commonly known as the cell imbalance issue. For the charging of battery packs, the cell imbalance not only early on terminates the charging process before all cells are fully charged, but also leads to different desired charging currents among cells. In this paper, based on the advancement in reconfigurable battery systems, we demonstrate how to utilize system reconfigurability to mitigate the impact of cell imbalance on an efficient charging process. With the proposed reconfiguration-assisted charging (RAC), cells in the system are categorized according to their real-time voltages, and the charging process is performed in a category-by-category manner. To charge cells in a given category, a graph-based algorithm is presented to charge cells with their desired charging currents, respectively. We evaluate RAC through both experiments and simulations. The results demonstrate that the RAC increases the capacity charged into cells by about 25% and yields a dramatically reduced variance.

Index Terms—Battery charging, cell imbalance, reconfigurable battery packs.

I. INTRODUCTION

LARGE-SCALE battery systems play critical roles in grids, electric vehicles, power backup systems, airplane

L. He is with the University of Michigan, Ann Arbor, MI 48109 USA, and also with the Key Laboratory of Computer Network and Information Integration (Southeast University), Ministry of Education, Nanjing 210096, China.

L. Kong is with Shanghai Jiaotong University, Shanghai 200240, China.

S. Lin is with Beijing Jiaotong University, Beijing 100044, China (e-mail: sylin@bjtu.edu.cn).

S. Ying is with the Singapore University of Technology and Design, Singapore 487372.

Y. Gu is with IBM Research, Austin, TX 78758 USA.

T. He is with Shanghai Jiaotong University, Shanghai, China, and also with the University of Minnesota, Minneapolis, MN 55455 USA.

C. Liu is with the University of Texas at Dallas, Dallas, TX 75080 USA.

Color versions of one or more of the figures in this paper are available online at http://ieeexplore.ieee.org.

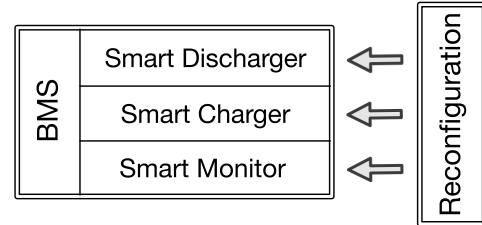Digital Object Identifier 10.1109/TSG.2015.2450727

Fig. 1. BMS architecture in reconfigurable battery packs.

electrical systems, etc. While such large systems are able to provide powerful energy supply, they also introduce new challenges, among which, the cell imbalance issue is one of the most critical problems [2]–[4].

Ideally, cells in a battery system should have similar characteristics. However, due to various reasons such as manufacturing difference, cell aging, etc., the cells' characteristics demonstrate significant dynamics over their usage [5]. The cell imbalance becomes more severe for large-scale battery systems, because many such systems can simultaneously support multiple loads with different energy requirements [3], [6], indicating cells in the system may have different discharge conditions.

The performance of unbalanced battery system is fundamentally limited by the weakest cell, to avoid issues such as thermal runaway [7], [8]. This is particular critical for cells connected in series, because the strength of a cell string is only as strong as the weakest cell. Thus, the imbalance among seriesly connected cells—commonly reflected by the variance among their open-circuit voltages (OCVs, i.e., the voltage between the cell terminals with no load applied)—prevents them to fully supply their capacities or being charged fully [9].

Exploring the reconfigurability of battery packs[1] is a new dimension to improve the system performance [4], [11], [12], in which the connectivity among cells can be altered based on real-time system conditions such as cell OCVs [13], cell temperature [3], and load requirements [4]. Fig. 1 shows the architecture of the battery management system (BMS) in reconfigurable battery packs, covering the functionalities of discharging, charging, and monitoring. Many investigations focusing on the reconfiguration-assisted discharge of battery

[1]The system reconfiguration also applies to other energy systems such as photovoltaic arrays [10].

systems have been reported, with the objective of maximizing the energy efficiency [2], [6]. The reconfiguration-assisted battery monitoring is explored in [5]. Complementary to these existing works, in this paper, we explore how to use the offered system reconfigurability to improve the charge of lithium-ion battery systems.

The challenges in efficiently charging a large battery system reside in two aspects. First, for a given cell, the desired charging current relies on its real-time OCV and thus is various during the charging process—the temporal heterogeneity of desired charging current [7]. Second, for a given time instant during the charging process, the desired charging currents for different cells may be different due to cell imbalance—the spatial heterogeneity of desired charging current.

In this paper, we propose the reconfiguration-assisted charging RAC for large lithium-ion battery systems. RAC tackles the temporal heterogeneity of desired charging current via the adaptive system (re)configuration, and addresses the spatial heterogeneity of desired charging current via the OCV-based cell categorization. The main contributions of this paper include the following.

1) To the best of our knowledge, this paper is the first attempt to exploit system reconfigurability to achieve an efficient charging process for large battery systems.
2) We propose a novel cell categorization method based on their OCVs and the system hardware constraints, with which cells with similar OCVs (and thus desiring similar charging currents) are categorized into the same category.
3) To charge cells in a given category, we transform the problem of identifying the desired system configuration for the charging process to a path selection problem in the abstracted cell graph. We prove the NP-hardness of the problem, and propose a solution to obtain the near-optimal system configuration.
4) We evaluate RAC through both experiments and simulations. The results show RAC increases the charged capacities of cells by about 25% and dramatically reduce their variance.

Note that although RAC requires the OCVs of cells as the input, this is not a new requirement for battery pack management. For example, estimating the state-of-charge of cells via voltage sensing is one of the most classic approach to estimate the remaining capacity of cells (and thus the battery pack) [14], [15].

II. PRELIMINARIES

A. Reconfigurable Battery Systems

The concept and implementation of reconfigurable battery packs, in which the connectivity among cells can be altered based on the application requirements, have been attracting increasing research attentions. As proposed in [6], a reconfigurable battery pack can be captured by a weighted directed graph $\mathcal{G} = \{\mathcal{V}, \mathcal{E}, \mathcal{W}\}$, where:

1) each vertex in $\mathcal{V}$ represents a cell in the battery pack and thus $|\mathcal{V}| = n$; two more vertices representing the
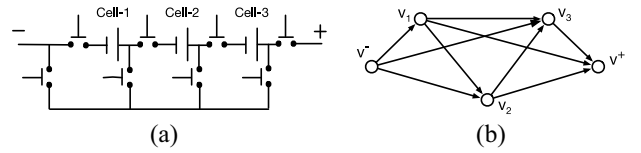

Fig. 2. Example on the battery pack graph representation. (a) Battery pack design. (b) Abstracted graph representation.
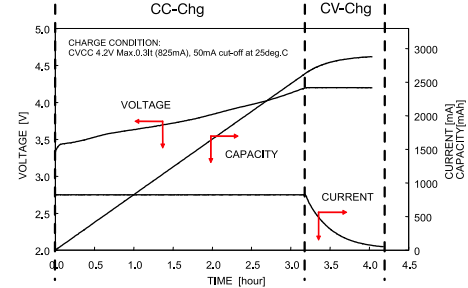

Fig. 3. Charging chart for Panasonic NCR18650 cells [17].

output terminals of the battery pack are further added in the graph[2];
2) $\mathcal{E}$ reflects how cells can be connected to each other and thus captures the system reconfigurability: an edge $v_i \to v_j \in \mathcal{E}$ if and only if the current can flow from v_i to v_j without passing through other cells;
3) the weight set $\mathcal{W}$ on the vertices captures the cell OCVs.

Fig. 2 illustrates an example of the graph representation of a three-cell reconfigurable battery pack according to [16]. With this battery pack, we can draw the current by connecting cell 1–3 in series. Correspondingly, directed edges $v^- \to v_1$, $v_1 \to v_2$, $v_2 \to v_3$, and $v_3 \to v^+$ exist in its graph representation.

The real-time monitoring of cells' OCVs is a fundamental functionality of BMS, and is the foundation for many other functions such as cell SoC estimation [14], [15]. We will explain how to obtain such information in Section III.

B. Heterogeneity of Desired Charging Currents

The heterogeneity of desired charging currents of cells is a critical challenge to efficiently charge lithium-ion battery packs, which comes from two aspects.

First, for a given cell, its desired charging current relies on its real-time OCVs—the temporal heterogeneity of desired charging current. As an illustrative example of the OCV-dependent charging currents, Fig. 3 plots the desired charging process of the Panasonic NCR18650 lithium-ion cells [17]. During the early phase of the charging process, the cell desires to be charged with a relatively large constant current (e.g., about 0.825 A in Fig. 3), referring to as the constant current charging (CC-Chg) phase. Then when cell's OCV reaches a certain level (e.g., about 4.19 V), the charging process switches to the constant voltage charging (CV-Chg) phase, during which the cell is charged with a constant voltage and

---

[2]Note that for many existing battery packs, the charging terminals can be directed connected to any cells via the backbone power buses [8]. We assume this full connectivity of charging terminals in the rest of this paper.
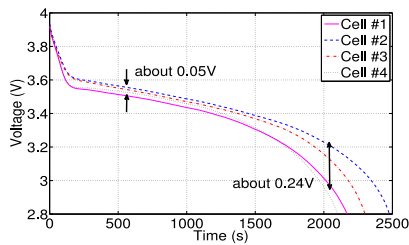
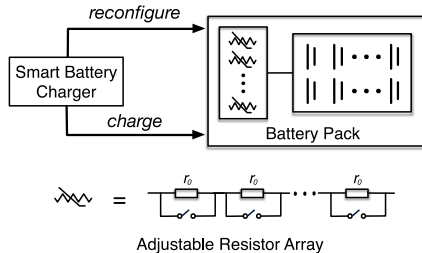Fig. 4. Voltage curves when discharging four cells in a battery pack for a Lenovo Thinkpad X220i laptop.

Fig. 5. System model overview.

the charging current decreases till the cell's OCV reaches the fully charged level.[3]

Second, cells in the battery pack may have different OCVs due to the imbalance issue. To clearly illustrate the cell imbalance issue, we dissembled a battery pack used in the Lenovo Thinkpad X220i laptop and discharged the four cells in it individually. The voltage curves of the four cells during discharge are plotted in Fig. 4, and obvious difference in cell voltages can be observed, e.g., as large as 0.24 V. Because of the different cell OCVs, for cells connected in series, their charging needs to be terminated when any of the cells reaches its voltage upper boundary to avoid over-charge [3], leading to the consequence that not all cells can be fully charged. Furthermore, because of the different OCVs, cells in the pack may desire different charging currents—the spatial heterogeneity of desired charging current. However, most off-the-shelf multicell chargers treat cells identically, e.g., the LP2952-based three-cell charger from TI always charges cells with the same current [19]. This unified charging current deviates cells' actual charging currents from their respectively desired level, degrading the charging process [20]. When the actual charging current is too large, cells cannot effectively accept all the provided charge, reducing the charging efficiency. Furthermore, an over-large charging current easily overheats cells and causes the thermal runaway issue [18]. On the other hand, an over-small charging current clearly prolongs the charging process and is not preferred by end-users [20].

C. System Model

In this paper, we tackle the efficient charging of large-scale battery systems by exploiting their reconfigurability. We consider the system model as shown in Fig. 5—besides imposing a

[3]Note that although the specific current and voltage (e.g., 0.825 A and 4.19 V) are only for the NCR18650 lithium-ion cells, the CC-Chg and CV-Chg phases are commonly adopted by all lithium-ion cells. The detailed explanation on charging lithium-ion cells can be found in [18].
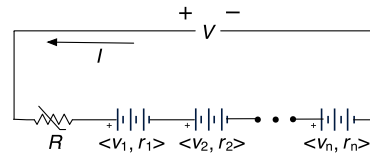

Fig. 6. Charging cells in series.

constant dc charging voltage V to a N-cell reconfigurable battery pack,[4] the smart charger, a module of the BMS in Fig. 1, also adjusts the configuration of cells according to their real-time OCVs to achieve the desired charging process, e.g., the one shown in Fig. 3.

Note that in practice, the desired charging process may be described by a range of charging currents instead of specific values. For example, a cell with 3.4 V OCV may desire to be charged with current in the range of 0.5–0.7 A. In such cases, we need to first determine which current is the most desirable, e.g., by jointly considering the charging time, power, etc. In the rest of this paper, we assume the specific optimal charging process is given.

To facilitate the fine-grained control over the charging current, we introduce a set of adjustable resistor arrays (with unit resistor r_0) into the system, with which we can adjust the size of resistance used and thus control the charging current. Two additional questions with regard to these resistor arrays are: 1) how to minimize the energy loss on resistors and 2) how many resistor arrays are needed and how large should each of them be. We will elaborate the two questions in Sections V and VI-B, respectively.

III. DESIGN PRINCIPLE

For cells connected in series (i.e., a cell string), the voltage they provide is the sum of their individual voltages and when charging, each cell has the same charging current. This fact inspires us the basic design principle of RAC.

Let us consider the example shown in Fig. 6. If a subset of x cells in the system are connected in series along with a resistor R, then with a charging voltage V, the charging current of these cells can be calculated as

$$I = \left(V - \sum_1^x v_i\right) \bigg/ \left(\sum_1^x r_i + R\right) \tag{1}$$

where v_i and r_i are the OCV and internal resistance of the ith cell, both of which are diverse during the charging process [20]. Clearly, we need the real-time v_i and r_i to achieve an efficient charging process.

The terminal voltages of cells (i.e., the voltage between the cell terminals with load applied) and their charging currents can be monitored by equipping voltage/current sensors on cells and is supported by most battery management systems [7], based on which cells' OCVs and internal resistance can be estimated. Note the terminal voltages of cells are different from their OCVs, due to the voltage drop caused by cell's

[4]Here, we assume the charger power is high enough for the charging process under consideration. This is feasible in practice because the capable charger is always selected according to the corresponding battery system.
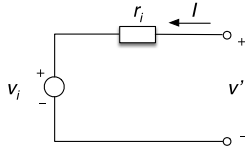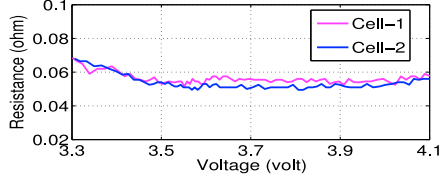
Fig. 7. Cell circuit model.

Fig. 8. Internal resistance of NCR18650 cell.

internal resistance. Considering the cell circuit model shown in Fig. 7, due to the voltage drop on the internal resistance r_i of cell i, the measured terminal voltage v' is higher than its OCV v_i, i.e., $v_i = v' - r_i \cdot I$. Assume the terminal voltage is v'_1 when charging the cell with current I_1, which changes to v'_2 when the charging current changes to I_2, we have

$$\begin{cases} v_i = v'_1 - r_i \cdot I_1 \\ v_i = v'_2 - r_i \cdot I_2. \end{cases}$$

This way, we can estimate v_i and r_i as

$$\begin{cases} v_i = \left(v'_2 \cdot I_1 - v'_1 \cdot I_2\right)/(I_1 - I_2) \\ r_i = \left(v'_1 - v'_2\right)/(I_1 - I_2). \end{cases} \quad (2)$$

However, in order to estimate v_i and r_i based on (2), we need to adjust cell's charging current (i.e., from I_1 to I_2). In RAC, this is achieved when switching system configurations during the charging process (Section VI-A).

With the estimated v_i and r_i and based on (1), the charging current of cells connected in series can be controlled by jointly considering: 1) how many (and which) cells should be adopted to compose the string (i.e., controlling $\sum_1^x v_i$ and $\sum_1^x r_i$) and 2) the amount of additional resistance connected along the string (i.e., controlling R).

For many types of cells, their internal resistances increase as being discharged [20]. For the charging process, this indicates a smaller r_i as v_i increases. However, for lithium-ion battery cells, the internal resistance is relatively stable during charging/discharging [7]. Fig. 8 shows our measurements on the internal resistance of a Panasonic NCR18650 lithium-ion cell during the charging process. We can see that the resistance is relatively stable (about 0.06 ohm) throughout the charging process. As a result, we simplify the presentation by assuming a stable cell internal resistance (denoted as r) during the charging process in the rest of the paper.[5]

Based on these observations, the proposed RAC consists of two steps. We first categorize cells according to their real-time OCVs, and then via system reconfiguration,[6] the

---

[5]Note that the cell internal resistance can be incorporated into RAC by assigning cell resistance as the second weight on the vertices of the cell graph.
[6]Note that although the reconfiguration lithium incurs additional energy consumption, this energy overhead is tolerable in the battery charging scenario, which can be supplied by the stable charging power.
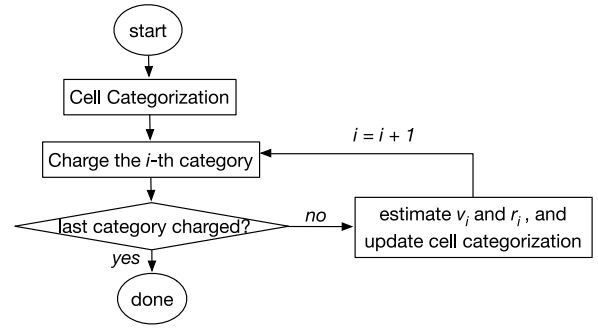

Fig. 9. RAC overview.

charging process is performed in a category-by-category manner. Fig. 9 presents an overview of RAC. We list several important notations used in the rest of this paper here and will introduce these two steps in the next two sections.

1) V: The charging voltage.
2) n: The number of cells in the battery pack.
3) m: The number of cell categories.
4) C_j ($j = 1, 2, \ldots, m$): The jth category of cells and $|C_j| = n_j$.
5) r: The internal resistance of cells.
6) v_i ($i = 1, 2, \ldots, n$): The OCV of the ith cell.
7) $\mathcal{G} = \{\mathcal{V}, \mathcal{E}, \mathcal{W}\}$: The battery pack's graph representation.
8) $\mathcal{G}_j = \{\mathcal{V}_j, \mathcal{E}_j, \mathcal{W}_j\}$: The graph representation of the cells in the jth category, and $\mathcal{G}_j \subseteq \mathcal{G}$.
9) $\mathcal{G}'_j = \{\mathcal{V}'_j, \mathcal{E}'_j, \mathcal{W}'_j\}$: The pruned graph based on $\mathcal{G}_j$ and $\mathcal{G}'_j \subseteq \mathcal{G}_j$.

IV. OCV-BASED CELL CLASSIFICATION

As cells connected in series have the same charging current, it is intuitive to compose a string only with cells demanding similar charging currents. In RAC, cells with similar OCVs (and thus desire similar currents) are organized into the same category, based on which the charging process is performed.

A. Basic Classification Idea

We discretize the range of cell OCVs into m intervals $\{[v_c^0, v_c^1], [v_c^1, v_c^2), \ldots, [v_c^{m-1}, v_c^m]\}$, where $v_c^0 = v_{\text{cutoff}}$ (i.e., the OCV defines cell's empty state) and $v_c^m = v_{\text{full}}$ (i.e., the cell OCV upon fully charged). For example, for the cell shown in Fig. 3, $v_{\text{cutoff}} \approx 3.20$ V and $v_{\text{full}} \approx 4.20$ V. Then m cell categories $\{C_1, C_2, \ldots, C_m\}$ are formed according to these intervals. Specifically, denoting the OCVs of the cells $\{b_1, b_2, \ldots, b_n\}$ in the pack as $\{v_1, v_2, \ldots, v_n\}$, we have

$$\forall i, j, \quad b_i \in C_j \leftrightarrow v_i \in \left[v_c^{j-1}, v_c^j\right).$$

After this classification, for cells in C_j, we use the median OCVs of all cells in this category to approximate their OCVs, denoted as $\hat{v}_c^j$, and use the corresponding desired charging current at $\hat{v}_c^j$ as their desired charging current, denoted as $\hat{I}_j$.

Intuitively, the desired charging current can be more accurately achieved with larger m. However, due to the hardware

constraints (e.g., the unit resistor r_0), over-high discretization granularity is not necessary.

B. Discretization During CC-Chg Phase

The unit resistor r_0 determines the minimum OCV changes we can differentiate by adjusting the added resistance. Let us consider an x-cell string with cell OCV $\hat{v}$. We will calculate the smallest $\hat{v}'$ ($\hat{v}' > \hat{v}$) that the system can accurately differentiate from $\hat{v}$ with a given r_0. From (1), we know

$$\begin{cases} \hat{v} = \left(V - x \cdot r \cdot \hat{I} - y \cdot r_0 \cdot \hat{I}\right)\big/ x \\ \hat{v}' = \left(V - x \cdot r \cdot \hat{I} - y' \cdot r_0 \cdot \hat{I}\right)\big/ x \end{cases} \tag{3}$$

where $\hat{I}$ is the desired charging current and is constant during the CC-Chg phase, and y and y' are the numbers of unit resistors involved in the string when the cell OCVs are $\hat{v}$ and $\hat{v}'$, respectively. Since $\hat{v}' > \hat{v}$, it is clear that $y' < y$. From (3), we know

$$\hat{v}' - \hat{v} = (y - y') \cdot r_0 \cdot \hat{I}\big/ x. \tag{4}$$

Because y, y', and x only take positive integer values, the minimal OCV increase is achieved when: 1) $y - y' = 1$ and 2) x reaches the maximal number of cells that can be connected in series in a feasible cell string. We refer a cell string to be feasible for the charging process if this string can be charged with a given charging voltage V. From (1), we know the maximum number of cells in a feasible string is

$$x_{\max} = \arg\max_x \left\{ (V - x \cdot \hat{v})/(x \cdot r + y \cdot r_0) = \hat{I} \right\}$$
$$\text{s.t. } \left\{ r, r_0, \hat{v}, V, \hat{I} \right\} > 0 \text{ and } \{x, y\} \in Z^+. \tag{5}$$

From (4) and (5), one can see that by adjusting the amount of included resistors, the smallest increase of OCV the system can detect is

$$\min\{\hat{v}' - \hat{v}\} = r_0 \cdot \hat{I}/x_{\max}. \tag{6}$$

As a result, starting from the cutoff voltage $v_c^0 = v_{\text{cutoff}}$, we iteratively discretize the OCV intervals during the CC-Chg phase according to (6), and achieves the highest accuracy the hardware can provide. This way, a smaller r_0 leads to a larger number of discretized intervals and thus a higher accuracy in achieving the desired charging current. However, a smaller r_0 also leads to a larger number of unit resistors in the resistor array, requiring a larger number of relays. We will further discuss the proper resistor array scale in Section VI-B.

C. Discretization During CV-Chg Phase

Different from the CC-Chg phase where the cell OCVs increases fast, the cell OCV increases slowly during the CV-Chg phase. For example, for the NCR18950 cell shown in Fig. 3, the CV-Chg phase starts when the cell OCV reaches about 4.19 V, and the entire charging process terminates when the cell OCV reaches 4.20 V, indicating a total OCV increase of only 0.01 V during the CV-Chg phase lasting about 1 h. On the other hand, the desired charging current decreases dramatically during this phase. This means higher discretization

granularity are needed to achieve good match with the desired charging currents. Therefore, we discretize the OCV intervals during the CV-Chg phase based on the highest measurement accuracy of the adopted voltage sensor.

V. CHARGING FOR EACH CATEGORY

After cell categorization, RAC charges the cells category-by-category according to the ascending order of OCVs. Specifically, cells in the first category are charged first until their OCVs evolve into the second interval, and thus these category-1 cells become category-2 cells. Then the cells in the (updated) second category are charged until their OCVs increase to the third interval. This process continues until all cells are fully charged. Next, we introduce how to identify the system configuration to efficiently charge cells in a given category.

A. Graph-Based Problem Transformation

Let us consider the case we are trying to identify the configuration to charge cells in the jth category C_j ($|C_j| = n_j$).

To charge the cells in C_j with the desired charging current $\hat{I}_j$, RAC identifies a set of cell strings involving each of these cells once and only once, and then by controlling the additional resistance added in each string, these cells can be optimally charged by connecting the strings in parallel. Note that these additionally involved resistance is also used in existing off-the-shelf battery chargers, e.g., LM2576 by TI [19]. Because these resistance introduces additional energy loss, we want to minimize the amount of involved resistance.

As mentioned in Section II, cells in C_j and their reconfigurability can be captured by a directed graph $\mathcal{G}_j = <\mathcal{V}_j, \mathcal{E}_j, \mathcal{W}_j>$. This way, any cell string in the battery pack can be captured by a simple path in the graph. Therefore, the problem of identifying cell strings to charge C_j can be transformed to identify a set of paths in $\mathcal{G}_j$ such that: 1) each vertex in $\mathcal{G}_j$ is involved in one and only one path, indicating the paths are disjoint and cover the vertex set $\mathcal{V}_j$ and 2) each path involves no more than $x_{\max}$ vertices.

Denote $\{P_1^j, P_2^j, \ldots, P_z^j\}$ as the identified disjoint paths. Further denote x_k and y_k ($k = 1, 2, \ldots, z$) as the number of vertices in P_k^j and the number of unit resistors added in P_k^j, respectively. For each b_i and P_k^j, we define the indicator variable

$$\alpha_{ik}^j = \begin{cases} 1 & \text{if } b_i \in C_j \text{ and } b_i \in P_k^j \\ 0 & \text{otherwise.} \end{cases}$$

This way, the problem can be formulated as

$$\min \quad \sum_{k=1}^z y_k \cdot r_0$$
$$\text{s.t.} \quad \forall k, \ \left(V - x_k \cdot \hat{v}_c^j\right)/(x_k \cdot r + y_k \cdot r_0) = \hat{I}_j$$
$$\forall i, \ \sum_{k=1}^z \alpha_{ik}^j = 1$$
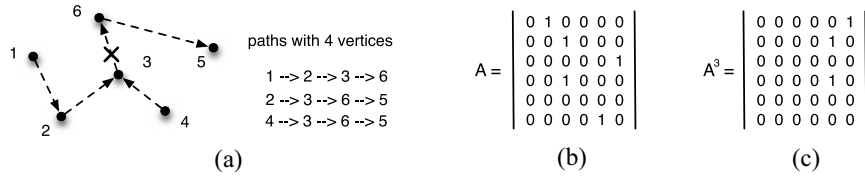$$\forall k, \ 1 \le x_k \le x_{\max}.$$

Fig. 10. Demonstration on the identification of cell strings. (a) Battery graph and all feasible paths. (b) Adjacent matrix of the battery graph. (c) 3rd power of the adjacent matrix.

Note the fact that $\sum_{k=1}^{z} x_k = n_j$, we have

$$\min \sum_{k=1}^{z} y_k \cdot r_0 \Leftrightarrow \min \sum_{k=1}^{z} \left(V - x_k \cdot \hat{v}_c^j - x_k \cdot r \cdot \hat{I}_j \right) \Big/ \hat{I}_j$$
$$\Leftrightarrow \min \left\{ z \cdot V - \hat{v}_c^j \cdot n_j - r \cdot \hat{I}_j \cdot n_j \right\}$$
$$\Leftrightarrow \min z. \tag{7}$$

As a result, in order to minimize the additional resistance adopted and thus the energy loss, we need to minimize the number of strings z. This is similar to the minimum path cover (MPC) problem in which we want to cover the vertex set of a given graph with the minimum number of paths [21], with the additional requirement that $x_k \leq x_{\max}$.

B. Two-Step Solution

The MPC problem not only helps to show the NP-hardness of our problem, but also inspires us a near-optimal solution with the following fact [22].

Observation 1: For directed acyclic graphs (i.e., a directed graph with no directed cycles), the MPC problem can be optimally solved in polynomial time.

Based on this observation, RAC prunes $\mathcal{G}_j$ to make it possible to leverage existing algorithms to identify the desired system configuration. The pruning of $\mathcal{G}_j$ needs to achieve two goals: 1) $\mathcal{G}_j$ needs to be pruned to an acyclic graph $\mathcal{G}_j'$ and 2) after applying existing MPC algorithms to $\mathcal{G}_j'$, the length of obtained paths (in terms of the number of involved vertices) is no more than $x_{\max}$.

1) Step I (Pruning the Graph): RAC achieves the above objectives by identifying and breaking all paths involving $(x_{\max}+1)$ vertices in $\mathcal{G}_j$. Denote $\mathbb{A} = \{\alpha_{ij}\}$ $(i, j = 1, 2, \ldots, N_j)$ as the adjacent matrix of $\mathcal{G}_j$—$a_{ij} = 1$ if there is an edge from vertex i to vertex j in $\mathcal{E}_j$ and $\alpha_{ij} = 0$ otherwise. The adjacent matrix has the following property.

Observation 2: For any given graph, the element a_{ij}^k in the kth power of its adjacent matrix (i.e., $\mathbb{A}^k$) is the number of paths from vertex i to j involving $(k+1)$ vertices.

As a result, any $\alpha_{ij}^{x_{\max}} \in \mathbb{A}^{x_{\max}}$ indicates the number of paths involving $(x_{\max}+1)$ vertices from vertex i to j. The time complexity for this matrix multiplication is $\mathcal{O}(x_{\max} \cdot N_j^{2.37})$ [23]. Then for each vertex pair (i, j) with $\alpha_{ij}^{x_{\max}} > 0$, we identify these $(x_{\max}+1)$-length paths from i to j by: starting from i, identify all its successor vertices, and then checking whether there exists a $x_{\max}$-vertex path from any of its successors to j. This process continues iteratively until all the $(x_{\max}+1)$-vertex paths from i to j are identified. The time complexity to identify these $(x_{\max}+1)$-vertex paths from i to j is $\mathcal{O}(d^{x_{\max}})$, where d is the vertex out-degree. As a result, a time of $\mathcal{O}(d^{x_{\max}} \cdot n_j^2)$

is needed to identify all the $(x_{\max}+1)$-vertex paths in $\mathcal{G}_j$. Note that for battery systems, the vertex out-degree d will not be large due to the consideration of system implementation complexity [6].

As an example, let us consider the subgraph (i.e., $\mathcal{G}_j$) shown in Fig. 10(a), and assume the feasible string can involve at most $x_{\max} = 3$ cells. The adjacent matrix $\mathbb{A}$ for the graph is shown in Fig. 10(b). Since each feasible path can involve at most three vertices, we calculate $\mathbb{A}^3$ as shown in Fig. 10(c). Because $\alpha_{1,6}^3 = 1$, we know there is one four-vertex path from vertices 1 to 6 [i.e., $1 \rightarrow 2 \rightarrow 3 \rightarrow 6$ as shown in Fig. 10(a)]. Similarly, because $\alpha_{2,5}^3 = 1$ and $\alpha_{4,5}^3 = 1$, we know another two four-vertex paths exists from vertices 2 to 5 and from vertices 4 to 5, respectively.

After identifying these $(x_{\max}+1)$-vertex paths, by removing at most one edge from them each, we can break these paths into two shorter paths each involving at most $x_{\max}$ vertices. The pruned graph after breaking these $(x_{\max}+1)$-vertex paths is denoted as $\mathcal{G}_j' = \{\mathcal{V}_j', \mathcal{E}_j', \mathcal{W}_j'\}$.

As we will see shortly, we want to minimize the number of removed edges when breaking these $(x_{\max}+1)$-vertex paths. To achieve this, for each edge $e_i \in \mathcal{E}_j$, we use the following indicator to denote whether it is involved in the kth path:

$$\beta_{ik} = \begin{cases} 1 & \text{if } e_i \text{ is on } P_k \\ 0 & \text{otherwise} \end{cases}$$

and further define another indicator to denote whether edge e_i is removed when breaking the $(x_{\max}+1)$-vertex paths

$$\eta_i = \begin{cases} 1 & e_i \in \mathcal{E}_j \text{ and } e_i \notin \mathcal{E}_j' \\ 0 & \text{otherwise.} \end{cases}$$

The problem of removing the minimum number of edges from $\mathcal{G}_j$ to break all $(x_{\max}+1)$-vertex paths is formulated as

$$\min \sum_{i=1}^{|\mathcal{E}_j|} \eta_i \quad \text{s.t.} \quad \forall k, \sum_{i=1}^{|\mathcal{E}_j|} \eta_i \cdot \beta_{ik} > 0. \tag{8}$$

This is a classic 0-1 integer linear programming with only one constraint and can be efficiently solved.

2) Step II (Identifying the Proper Configuration):

Theorem 1: $\mathcal{G}_j'$ is acyclic and has no path involving more than $x_{\max}$ vertices.

This theorem can be proved by contradiction and we do not include the proof here due to the space limit.

This way, we can apply existing MPC solutions, e.g., Hopcroft–Karp algorithm [24], to $\mathcal{G}_j'$ to obtain a set of paths based on which C_j can be efficiently charged. We have the following theorem on the near-optimality of the obtained configuration in terms of the number of cell strings.

Theorem 2: Denote z and z^* as the number of paths obtained by RAC and that for the optimal solution. Further denote u as the number of edges removed from $\mathcal{G}_j$ when breaking the $(x_{\max} + 1)$-vertex paths (i.e., $|\mathcal{V}_j| - |\mathcal{V}'_j| = u$), we have $z \leq z^* + u$.

This theorem is based on the observation that for any removed edge, it can at most connect two of the obtained paths into one longer path (this connected longer path may not be feasible anymore). As a result, if we add all these u removed paths back to $\mathcal{G}'_j$, the MPC number can be reduced at most by u, and thus the theorem follows.

From Theorem 2, we can see the number of removed edges bounds the near-optimality of RAC . This is the reason why we want to break the $(x_{\max} + 1)$-vertex paths by removing the fewest number of edges.

C. Amount of Additional Resistors

After identifying the cell strings, we need to determine the amount of resistance to be connected along each of the strings to achieve the desired charging current $\hat{I}_j$. For P_i with x_i vertices, we want to add a proper number of unit resistors to make the achieved charging current I as close as possible to $\hat{I}_j$

$$\min\left\{\left|I - \hat{I}_j\right|\right\}. \tag{9}$$

By substituting (1) into (9), we identify the number of added unit resistors by

$$\arg\min_{y_i}\left\{\left|\left(V - x_i \cdot \hat{v}_c^j\right)/(x_i \cdot r + y_i \cdot r_0) - \hat{I}_j\right|\right\}.$$

VI. PRACTICAL ISSUES AND FURTHER DISCUSSION

A. Estimating of Cell OCV and Resistance

For system safety concerns such as avoiding the instant arc flash caused by abrupt current changes [25], the charging process needs to be temporarily interrupted during the switching of system configurations, i.e., when switching from charging the jth category to charging the $(j + 1)$th category. This interruption of charging currents—reducing from I_j to 0 and then increases to I_{j+1}—offers the opportunity to estimate cells' OCVs and internal resistance according to (2).

B. Scale of Resistor Arrays

Clearly, an over-small scale resistor array may prevent to achieve the desired charging current when a large amount of resistance is required. On the other hand, an over-large scale is not necessary and only increases system complexity in vain. We next discuss the proper size of the resistor arrays. Note the scale of resistor arrays are not directly related to the energy loss on resistors, which on the other hand is determined by the amount of resistors that is actually connected along the strings during charging.

From (1), we know the number of unit resistors to be connected along a cell string is jointly determined by cells' OCVs (and thus their desired charging current) and the string size. Fig. 11 shows the resistance required during the charging process with a charging voltage of 30 V. We can see the largest amount of resistance is required when: 1) the smallest charging
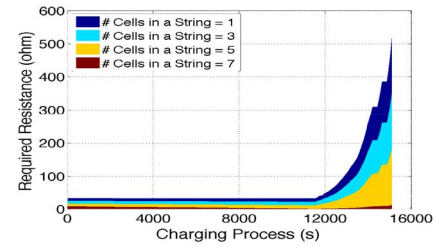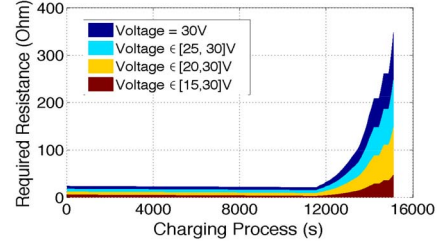

Fig. 11. Required resistance.

Fig. 12. Resistance with adjustable charging V.

current is required (i.e., during the final stage of the CV-Chg phase) and 2) the cell string consists of only one single cell. Thus for a given battery system, we can calculate the maximum required resistance $R_{\max}$ based on the corresponding charging voltage. With a unit resistance r_0, the number of unit resistors in each resistor array is $\lceil R_{\max}/r_0 \rceil$.

Once we know the size of individual resistor arrays, we can determine the number of these resistor arrays required in the system accordingly. During the charging process, if more than one cell strings require the same number of unit resistors, they can share the same resistor array by connecting these strings in parallel and then connect with the resistor array in series. As a result, only a single resistor array is needed for a specific number of required unit resistors. Thus, we can see that equipping the system with $\lceil R_{\max}/r_0 \rceil$ resistor arrays is enough to perform RAC.

C. Joint Control of Charging Voltage and Reconfiguration

A constant charging voltage from the charger is assumed in this paper, and additional resistance is used to control the charging current in finer granularity. As a result, a relatively large amount of resistance is required when the charging voltage is much larger than the voltage of to-be-charged cell strings, degrading the charging efficiency. A potential approach to reducing the amount of involved resistance is to jointly adjust the charging voltage and the system configuration, in compliance with the desired charging currents of cells. Fig. 12 plots the required resistance when the charging voltage can be adjusted with certain freedom. We can see a higher freedom in adjusting the charging voltage helps to reduced the amount of required resistance during the charging process and thus improves the energy efficiency. Here, we want to emphasize that RAC is compatible to the scenarios with controllable charging voltage—after determining the proper charging voltage, the problem regresses to what is exactly considered in this paper and RAC can be applied without any changes.

$$\begin{bmatrix} 0 & 0 & 1 & 0 & 1 & 1 & 0 & 0 \\ 1 & 0 & 0 & 1 & 0 & 0 & 1 & 0 \\ 0 & 1 & 0 & 0 & 1 & 0 & 0 & 1 \\ 1 & 0 & 1 & 0 & 0 & 1 & 0 & 0 \\ 1 & 1 & 0 & 0 & 0 & 0 & 0 & 1 \\ 0 & 1 & 0 & 0 & 1 & 0 & 1 & 0 \\ 1 & 0 & 0 & 1 & 0 & 0 & 0 & 1 \\ 0 & 0 & 1 & 0 & 0 & 1 & 1 & 0 \end{bmatrix}$$

Fig. 13. Reconfigurability of the eight-cell pack.

D. Overhead of Battery Pack Reconfiguration

The reconfiguration of battery packs is achieved by equipping switches in the pack and controlling their open/close states. This, besides offering a new dimension to improve system performance, also incurs additional overhead, in terms of the energy for switch operation, the delay for reconfiguration, and the physical size of switches, especially for large-scale battery packs.

A potential approach to reduce such overhead is to explore the module-level reconfigurability, instead of the cell-level as in this paper. Actually, this is a common approach in traditional nonreconfigurable battery packs. For example, the 23 kWh battery pack from A123 systems consists of multiple AMP20 energy modules [26]. This way, the number of switches required can be reduced and achieves a tradeoff between the reconfigurability and system complexity. The proposed RAC can be applied in the same way on such module-level reconfigurable battery packs. We will further investigate the optimal modularization of reconfigurable battery packs in our future work.

VII. EXPERIMENT EVALUATION

A. Experiment Methodology

Due to the lack of automatic testbed of reconfigurable battery packs, we evaluate RAC with an emulated battery pack consisting of eight NCR18650 cells, each with a nominal capacity of 2900mAh. The randomly generated system reconfigurability, represented by its adjacent matrix, is shown in Fig. 13.

We introduce a control parameter ϕ to capture the cell imbalance degree: the initial OCVs of cells are randomly generated (and achieved with the battery testing system) from

$$[v_{\text{cutoff}}, \ v_{\text{cutoff}} + \phi(v_{\text{max}} - v_{\text{cutoff}})] \quad (\phi \in [0, 1]) \quad (10)$$

where v_{cutoff} and v_{max} are 3.30 V and 4.20 V according to the charging chart of the NCR18650 cell shown in Fig. 3. In this way, a larger ϕ indicates higher unbalanced cells.

With a unit resistance of 2 Ω and a 0.002 V voltage sensor accuracy, the entire OCV range [3.30, 4.20] is divided into seven intervals: [3.30, 3.517), [3.517, 3.723), [3.723, 3.956), [3.956, 4.193), [4.193, 4.195), [4.195, 4.197), and [4.197, 4.20]. The first four intervals are for the CC-Chg phase and the latter three intervals are for the CV-Chg phase. The eight cells are then categorized based on their initial OCVs. According to the charging chart in Fig. 3, the corresponding desired charging currents for cells in these categories are 0.825, 0.825, 0.825, 0.825, 0.398, 0.177, and 0.084 A. We then apply RAC on the battery system to obtain the

TABLE I
INITIAL OCVs (V)

ϕ	#1	#2	#3	#4	#5	#6	#7	#8
0.1	3.353	3.306	3.377	3.370	3.352	3.356	3.331	3.361
0.3	3.473	3.439	3.456	3.372	3.394	3.437	3.533	3.336
0.5	3.560	3.548	3.520	3.360	3.460	3.432	3.556	3.580
0.7	3.812	3.596	3.214	3.639	3.618	3.920	3.862	3.805
0.9	3.710	4.044	3.960	4.072	3.862	3.428	3.995	4.058

TABLE II
DELIVERED CAPACITIES (mAh)

ϕ	Cell	#1	#2	#3	#4
0.1	Reconf.	2619.5	2636.8	2617.6	2670.5
	Non-Reconf.	2508.5	2607.7	2613.7	2660.7
0.3	Reconf.	2607.6	2560.6	2608.6	2660.0
	Non-Reconf.	2597.3	627.8	2576.8	2459.0
0.5	Reconf.	2616.4	2628.5	2611.1	2665.2
	Non-Reconf.	2622.3	2510.3	2492.6	2304.3
0.7	Reconf.	2606.5	2614.8	2595.6	2646.3
	Non-Reconf.	2597.9	2046.1	857.7	2253.8
0.9	Reconf.	2617.9	2633.0	2610.9	2670.2
	Non-Reconf.	1566.4	2580.1	2340.3	2663.3

ϕ	Cell	#5	#6	#7	#8
0.1	Reconf.	2706.3	2582.0	2657.9	2621.9
	Non-Reconf.	2611.6	2575.6	2593.6	2606.5
0.3	Reconf.	2694.5	2567.7	2644.4	2609.6
	Non-Reconf.	2432.7	2458.2	2647.7	2276.7
0.5	Reconf.	2704.2	2577.6	2650.8	2611.8
	Non-Reconf.	2364.4	2222.4	2526.6	2610.6
0.7	Reconf.	2682.0	2555.1	2632.6	2593.6
	Non-Reconf.	1821.6	2553.6	2499.8	2300.0
0.9	Reconf.	2714.4	2579.4	2649.9	2606.7
	Non-Reconf.	2140.1	541.3	2501.5	2614.3

detailed charging profile for each cell, which is in the form of $<c_i, v_i>$ $(i = 1, 2, \ldots)$—charge the cell with current c_i until its voltage reaches v_i. Finally, the battery testing system is adopted to actually perform the charging according to these profiles.

As a baseline, we explore a nonreconfigurable eight-cell system with the configuration of $4S2P$: two cell strings (i.e., $B_1 \rightarrow B_2 \rightarrow B_3 \rightarrow B_4$ and $B_5 \rightarrow B_6 \rightarrow B_7 \rightarrow B_8$) are connected in parallel. With this fixed configuration, for system safety, the charging current on each string is determined by the smallest desired charging current of the four cells in the string, and the charging process is terminated when any of these 4 cells reaches its full OCV [3], [8].

After the charging process finishes, we discharge the cells with a constant current of 200 mA till their voltages decrease to 3.30 V. The delivered capacity during discharging is recorded and taken as the evaluation metric.

B. Experiment Results

We explore 5 cases with varying ϕ, and the cells' initial OCVs are shown in Table I. The delivered capacity with RAC and the nonreconfigurable baseline are listed in Table II.

We can see after charged according to RAC, about 2600 mAh capacity can be delivered for each cell in all explored cases, and the delivered capacity are more stable in terms of both average and standard deviations, when compared with the nonreconfigurable baseline. Note variance still exists because of: 1) the difference in the initial state of cells and 2) the high voltage sensitivity during the CV-Chg phase.
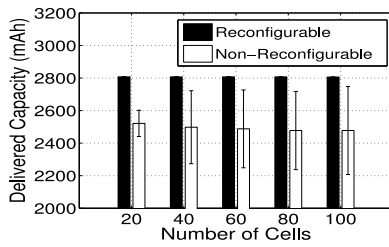
Fig. 14. Capacity versus # of cells.

We also tested the delivered capacity (with 0.2 A discharge current) after charging the cells with the associated commercial charger, similar results (about 2600 mAh) are obtained as with RAC. Note that the charge of these cells with the commercial charger is performed individually rather than in-batch as with RAC.

The delivered capacity decreases as ϕ increases with the nonreconfigurable baseline, e.g., from an average delivered capacity of 2597.2 mAh with $\phi = 0.1$ decreased to 2118.4 mAh with $\phi = 0.9$, indicating the cells are only charged to about 73% of their nominal capacity on average. This is mainly caused by two reasons. First, the charging process has to be terminated when any cell in the string reaches its full OCV for system safety consideration, indicating other cells may not be fully charged. Second, the charging current on a cell string is determined by the smallest desired current of the four cells, which may reduce the charging efficiency of other cells when different charging currents are desired.

VIII. Simulation Evaluation

We simulate a battery system consisting of 20–100 NCR18650 cells. The system reconfigurability, described by the average vertex out-degree d in its corresponding graph representation, varies from 1 to 5. The neighbors of a given cell are randomly selected. Same as in the experiment, the initial OCVs of cells are randomly generated according to (10). With a unit resistor of 2 Ω and voltage sensor accuracy of 0.002 V, the entire voltage range [3.30, 4.20] is divided into seven intervals. We also simulate nonreconfigurable battery systems with the configuration of $N/4S4P$ as baselines (i.e., four parallel connected cell strings each consisting of $N/4$ cells). The desired charging currents and corresponding OCVs are obtained from the NCR18650 data sheet as shown in Fig. 3. The results reported are based on 50 simulation runs.

To verify the impact of system scale on RAC, we vary the number of cells in the system from 20 to 100 cells with a reconfigurability of 3 and $\phi = 0.5$, and apply RAC to charge the system. The cell capacities after the completion of the charging processes (with RAC and for the nonreconfigurable system, respectively) are plotted in Fig. 14. One can see that in terms of the charged capacity, RAC achieves stable and competitive performance for all explored cases. On the other hand, in the nonreconfigurable system, the charged cell capacities decrease as the system scale increases. This is because the charging process in this case has to be terminated when any of these cells reaches its full OCV, leaving other cells insufficiently charged.

IX. Conclusion

In this paper, we have demonstrated the effectiveness of RAC, which achieves a high-efficiency charging process for large-scale lithium-ion battery systems via the exploration of system reconfigurability. By categorizing cells according to their OCVs, RAC performs charging in a category-by-category manner. A graph-based algorithm has been proposed to identify the system configuration to charge cells in a given category. The performance of RAC has been verified through both experiments and simulations.

Resistance arrays are used in RAC to facilitate the fine-grained current control. In our future work, we will explore other approaches to control the charging voltage/current (e.g., via dc–dc conversion) to further improve the RAC process.

References

[1] L. He *et al.*, "Reconfiguration-assisted charging in large-scale lithium-ion battery systems," in *Proc. ACM/IEEE ICCPS*, Berlin, Germany, 2014, pp. 60–71.

[2] H. Kim and K. G. Shin, "Scheduling of battery charge, discharge, and rest," in *Proc. RTSS*, Washington, DC, USA, 2009, pp. 13–22.

[3] H. Kim and K. G. Shin, "On dynamic reconfiguration of a large-scale battery system," in *Proc. RTAS*, San Francisco, CA, USA, 2009, pp. 87–96.

[4] F. Jin and K. G. Shin, "Pack sizing and reconfiguration for management of large-scale batteries," in *Proc. ICCPS*, Beijing, China, 2012, pp. 138–147.

[5] H. Kim and K. G. Shin, "Efficient sensing matters a lot for large-scale batteries," in *Proc. ICCPS*, Chicago, IL, USA, 2011, pp. 197–205.

[6] L. He *et al.*, "Exploring adaptive reconfiguration to optimize energy efficiency in large-scale battery systems," in *Proc. RTSS*, Vancouver, BC, Canada, 2013, pp. 118–127.

[7] D. Andrea, *Battery Management Systems for Large Lithium-ion Battery Packs*. Boston, MA, USA: Artech House, 2010.

[8] H. Kim and K. G. Shin, "Dependable, efficient, scalable architecture for management of large-scale batteries," in *Proc. ICCPS*, Stockholm, Sweden, 2010, pp. 178–187.

[9] T. Kim, W. Qiao, and L. Qu, "Series-connected self-reconfigurable multicell battery," in *Proc. APEC*, Fort Worth, TX, USA, 2011, pp. 1382–1387.

[10] G. Spagnuolo *et al.*, "Control of photovoltaic arrays: Dynamical reconfiguration for fighting mismatched conditions and meeting load requests," *IEEE Ind. Electron. Mag.*, vol. 9, no. 1, pp. 62–76, Mar. 2015.

[11] L. He, S. Ying, and Y. Gu, "Reconfiguration-based energy optimization in battery systems: A testbed prototype," in *Proc. IEEE RTSS*, Vancouver, BC, Canada, 2013, pp. 60–71.

[12] L. He, Y. Gu, C. Liu, T. Zhu, and K. G. Shin, "SHARE: SoH-aware reconfiguration to enhance deliverable capacity of large-scale battery packs," in *Proc. ACM/IEEE ICCPS*, Seattle, WA, USA, 2015, pp. 169–178.

[13] T. Kim, W. Qiao, and L. Qu, "A series-connected self-reconfigurable multicell battery capable of safe and effective charging/discharging and balancing operations," in *Proc. APEC*, Orlando, FL, USA, 2012, pp. 2259–2264.

[14] S. Lee, J. Kim, J. Lee, and B. Cho, "State-of-charge and capacity estimation of lithium-ion battery using a new open-circuit voltage versus state-of-charge," *J. Power Sources*, vol. 185, no. 2, pp. 1367–1373, 2008.

[15] M. Coleman, C. K. Lee, C. Zhu, and W. Hurley, "State-of-charge determination from EMF voltage estimation: Using impedance, terminal voltage, and current for lead-acid and lithium-ion batteries," *IEEE Trans. Ind. Electron.*, vol. 54, no. 5, pp. 2550–2557, Oct. 2007.

[16] B. Lawson, "A software configurable battery," in *Proc. EVS26 Int. Battery Hybrid Fuel Cell Elect. Veh. Symp.*, Los Angeles, CA, USA, 2012, pp. 1–12.

[17] *Panasonic NCR18650 Li-ion Battery*. [Online]. Available: http://industrial.panasonic.com/www-data/pdf2/ACA4000/ACA4000CE240.pdf, accessed 2015.

[18] R. Garcia-Valle and J. A. P. Lopes, Eds., "Electric vehicle integration into modern power networks," in *Power Electronics and Power Systems*, New York, NY, USA: Springer, 2013.

[19] *LM2576, LM3420, LP2951, LP2952*. [Online]. Available: http://www.ti.com/lit/an/snva557/snva557.pdf, accessed 2015.

[20] D. Linden and T. B. Reddy, *Handbook of Batteries*, 3rd ed. New York, NY, USA: McGraw-Hill, 2001.

[21] S. C. Ntafos and S. L. Hakimi, "On path cover problems in digraphs and applications to program testing," *IEEE Trans. Softw. Eng.*, vol. 5, no. 5, pp. 520–529, Sep. 1979.

[22] L. R. Ford and D. R. Fulkerson, *Flows in networks*. Princeton, NJ, USA: Princeton Univ. Press, 1962.

[23] T. H. Cormen, C. E. Leiserson, R. L. Rivest, and C. Stein, *Introduction to Algorithms*. Cambridge, U.K.: MIT Press, 2001.

[24] J. E. Hopcroft and R. M. Karp, "An $n^{5/2}$ algorithm for maximum matchings in bipartite graphs," *SIAM J. Comput.*, vol. 2, no. 4, pp. 225–231, 1973.

[25] *The Basics of Arc Flash*. [Online]. Available: http://www.geindustrial.com/sites/geis/files/gallery/The-Basics-of-Arc-Flash-Article_GE_Industrial_Solutions_0.pdf, accessed 2015.

[26] *AHR32113 Power Modules*. [Online]. Available: http://www.a123systems.com, accessed 2015.

Shaodong Ying (M'13) received the B.S. and M.S. degrees in control science and engineering from Zhejiang University, Hangzhou, China, in 2001 and 2006, respectively.

He is currently a Research Assistant with the Singapore University of Technology and Design, Singapore. His current research interests primarily include large scale battery management system, energy management system, and wireless sensor networks.

Dr. Ying is a member of the IEEE Communications Society.

Liang He (S'09–M'12) received the B.Eng. degree from Tianjin University, Tianjin, China, in 2006, and the Ph.D. degree from Nankai University, China, in 2011, both in computer science.

From 2009 to 2011, he was a Visiting Research Student with the University of Victoria, Victoria, BC, Canada. He is currently a Research Fellow with the University of Michigan, Ann Arbor, MI, USA.

Dr. He was a recipient of the Best Paper Award from the IEEE International Conference on Wireless Communications and Signal Processing 2011, the IEEE Global Communications Conference (GLOBECOM) 2011, QShine 2015, and the Best Paper Candidate from IEEE GLOBECOM 2014.
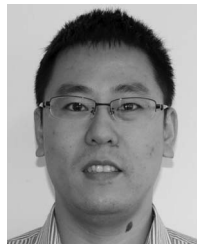
Yu (Jason) Gu (M'11) received the Ph.D. degree from the Department of Computer Science and Engineering, University of Minnesota, Minneapolis, MN, USA, in 2010.

He was an Assistant Professor with the Singapore University of Technology and Design, Singapore, from 2010 to 2014. He is currently a Research Scientist with IBM Research, Austin, TX, USA. He has authored and co-authored over 70 papers in premier journals and conferences. His publications have been selected as graduate course materials by over ten universities in the United States and other countries.
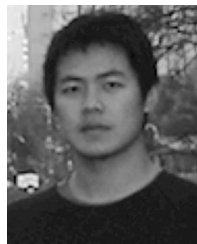
Tian He (SM'12) received the Ph.D. degree in computer science from the University of Virginia, Charlottesville, VA, USA.

He is currently an Associate Professor with the Department of Computer Science and Engineering with the University of Minnesota–Twin Cities, Minneapolis, MN, USA. His current research interests include wireless sensor networks, intelligent transportation systems, real-time embedded systems, and distributed systems, supported by the National Science Foundation (NSF), IBM, Microsoft, and other agencies. He has authored and co-authored over 190 papers in premier wireless network journals and conferences with over 15 000 citations and an H-index of 49.

Dr. He was a recipient of the George W. Taylor Distinguished Research Award, the NSF CAREER Award, McKnight Land-Grant Professorship, and five best paper awards. He served a few General/Program Chair positions in international conferences and on many program committees. He currently serves as an Editorial Board Member for six international journals including the *ACM Transactions on Sensor Networks* and the IEEE TRANSACTION ON COMPUTERS.

Linghe Kong (S'09–M'13) received the B.E. degree in automation from Xidian University, Xi'an, China, in 2005, the Dipl.Ing. degree in telecommunication from TELECOM SudParis, Évry, France, in 2007, and the Ph.D. degree in computer science from Shanghai Jiao Tong University, Shanghai, China, in 2012.

He is currently a Post-Doctoral Research Fellow with Shanghai Jiao Tong University.

Cong Liu (M'13) received the Ph.D. degree in computer science from the University of North Carolina at Chapel Hill, Chapel Hill, NC, USA, in 2013.

He is currently an Assistant Professor with the Department of Computer Science, University of Texas at Dallas, Dallas, TX, USA. His current research interests include real-time and embedded systems, cyber-physical systems, and mobile and cloud computing. He has authored and co-authored over 30 papers in premier journals and conferences.

Dr. Liu was a recipient of the Best Student Paper Award from the 30th IEEE Real-Time System Symposium, and the Best Paper Award from the 17th International Conference on Embedded and Real-Time Computing Systems and Applications.

Siyu Lin (S'09–M'14) received the B.E. and Ph.D. degrees from Beijing Jiaotong University, Beijing, China, in 2007 and 2013, respectively, both in electronic engineering.

From 2009 to 2010, he was an Exchange Student with the Universidad Politecnica de Madrid, Madrid, Spain. From 2011 to 2012, he was a Visiting Student with the University of Victoria, Victoria, BC, Canada. He is currently a Lecturer with Beijing Jiaotong University.